NJC

ROYAL SOCIETY OF CHEMISTRY

PAPER

View Article Online
View Journal

Cite this: DOI: 10.1039/d6nj00558f

Structural and computational evidence of rare synergic N(amide)H···Au(I) and N(amidate)···Au(I) secondary bonding interactions

Laura Coconubo-Guio,[a] Sonia Moreno,[a] Giacomo Picci,[b] Miguel Monge,[a] José M. López-de-Luzuriaga,[a] M. Elena Olmos,*[a] Claudia Caltagirone*[b] and Vito Lippolis*[b]

Received 12th February 2026,
Accepted 20th April 2026

DOI: 10.1039/d6nj00558f

rsc.li/njc

This work focusses on weak NH···Au(I) non-covalent interactions (NCIs), a subject of ongoing debate. It reports the synthesis and characterization of new gold(I) complexes featuring the pincer ligand *N*,*N*′-bis{(2-diphenylphosphanyl)phenyl}-2,6-pyridinedicarboxamide (**L**). Rare examples of N(amide)H···Au(I) interactions in different coordination environments are examined. In the neutral complex [Au($\mathbf{L}_{-H}$)] (**3**), both a directional N(amide)H···Au(I) contact consistent with a metal-centered hydrogen bond and an uncommon secondary N(amidate)···Au(I) interaction are identified, highlighting their relevance for future structural and computational analyses.

Introduction

Non-covalent interactions (NCIs), including hydrogen,[1] halogen[2] and chalcogen bonding,[3] play an essential role in supramolecular and coordination chemistry, where they govern key concepts such as preorganization, complementarity, cooperativity, selectivity and discrimination.[4] Their ability to influence structure, stability and reactivity has made them powerful tools for rational molecular design across fields ranging from crystal engineering to catalysis. Recent literature continues to emphasise the centrality of NCIs in dictating the behaviour of coordination compounds and the diversity of weak bonding patterns accessible to transition metals.[5] Such studies highlight the need for a deeper understanding of special bonding motifs already known in coordination chemistry and their structural and functional consequences.

Within this broad context, weak interactions of the type M···H–X (X = C, N, O, and halogens) involving electron-rich transition metals have attracted increasing interest. These contacts, frequently interpreted as metal-centred hydrogen bonds,[6–8] are relevant to fundamental processes, such as the protonation of transition metals to form metal hydrides, and to X–H activation in catalysis. Their identification, however, is complicated by the coexistence of multiple NCIs, geometric constraints and metal-dependent electronic effects.

Gold(I) provides a particularly compelling platform for investigating such interactions. Its closed-shell d^{10} configuration, strong relativistic effects, high electronegativity and preference for linear coordination endow gold(I) compounds with a remarkable efficiency in both heterogeneous and homogeneous catalyses[9–11] and enable unconventional secondary bonding. Despite possessing characteristics that should favour X–H···Au(I) hydrogen bonding, the capacity of gold(I) to function as a true hydrogen-bond acceptor remains a subject of ongoing debate.[12–18] Distinguishing authentic Au···H hydrogen bonds from short contacts constrained by packing forces, competing NCIs, including metallophilic interactions, or the ligand framework is particularly challenging.[12,19] Spectroscopic signatures typical of hydrogen bonding are often ambiguous in gold complexes due to the relativistic and electronic environment at the metal centre, further complicating reliable identification.[20,21] Consequently, only limited well-supported examples exist, underscoring the need for new systems that expand the structural diversity available for analysis.

Advancing this field requires systematic exploration of gold(I) complexes capable of supporting putative X–H···Au(I) interactions, allowing the identification of consistent geometric or electronic trends that clarify their origin and significance. Recent contributions show that *ortho*-aminophenylphosphines constitute promising scaffolds for probing such weak interactions, as they combine strong electron-donating phosphorus donors with strategically positioned N–H groups oriented toward the metal centre.[21,22] These ligand platforms offer an

[a] *Departamento de Química, Instituto de Investigación en Química de la Universidad de La Rioja (IQUR), Universidad de La Rioja, Complejo Científico Tecnológico, 26006-Logroño, Spain. E-mail: m-elena.olmos@unirioja.es*
[b] *Dipartimento di Scienze Chimiche e Geologiche, Università degli Studi di Cagliari, S.S. 554 Bivio per Sestu, 09042 Monserrato (CA), Italy. E-mail: lippolis@unica.it, ccaltagirone@unica.it*

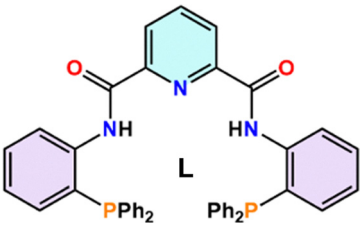

Scheme 1 Molecular structure of *N*,*N*′-bis{(2-diphenylphosphanyl)-phenyl}-2,6-pyridinedicarboxamide (**L**).

opportunity to examine how the coordination environment and ligand flexibility influence the emergence of weak, metal-centred NCIs.

Herein, we investigate the coordination chemistry of gold(I) with the flexible pincer ligand *N*,*N*′-bis{(2-diphenylphosphanyl)-phenyl}-2,6-pyridinedicarboxamide (**L**) (Scheme 1), designed to probe N(amide)H···Au(I) interactions across distinct coordination environments. The conformational adaptability of **L** enables access to structural arrangements not attainable with more rigid pincer frameworks, providing an ideal platform for identifying diverse weak interactions around gold. In this work, structural and computational analyses reveal rare examples of N(amide)H···Au(I) hydrogen bond-like interactions together with an unusual secondary N(amidate)···Au(I) contact. These findings expand the limited catalogue of existing special bonding motifs in gold(I) coordination chemistry and provide new insights into the fundamental characteristics governing weak, metal-centred NCIs.

Results and discussion

Synthesis and characterization

The pincer ligand **L** was synthesised following the procedures reported by B. L. Feringa[23] and Y. Liu,[24] by reacting 2,6-pyridinedicarbonyl dichloride with 2-(diphenylphosphino)aniline in a 1 : 2 molar ratio in THF under a nitrogen atmosphere (see the Experimental section). A slight excess of triethylamine was added to promote partial deprotonation of the aniline, thereby facilitating the formation of the amide groups.

Reaction of **L** with [AuCl(tht)] (tht = tetrahydrothiophene) in 1 : 2 and 1 : 1 molar ratios in CH_2Cl_2 afforded white solid powders corresponding to the formulation [$(AuCl)_2$(**L**)] (**1**) and [AuCl(**L**)] (**2**), respectively (see Fig. S1 and S2 for mass spectra in the supplementary information (SI)). Both compounds are moderately stable in air and moisture at room temperature. They are soluble in organic solvents such as acetone and in chlorinated solvents such as CH_2Cl_2 and $CHCl_3$, but insoluble in *n*-hexane and diethyl ether. Molar conductivity measurements in acetone solutions (5×10^{-4} M) indicate that both behave as non-electrolytes, consistent with their neutral nature, showing values of 4.1 (**1**) and 3.2 (**2**) Ω^{-1} cm^2 mol^{-1}, respectively. The infrared spectra of **1** and **2** display bands corresponding to the stretching vibration of the amide group in the ranges of 3017–2946 cm^{-1} and 3201–3055 cm^{-1}, respectively (Fig. S3 and S4), which are only slightly shifted with respect to the corresponding vibration of the free ligand (3338–3275 cm^{-1}).[24] This observation, together with the presence of a single, markedly low-field-shifted resonance in the $^{31}P\{^1H\}$-NMR spectrum ($CDCl_3$) of the two compounds [δ_P = 23.98 ppm for **1**, 34.97 ppm for **2**, −19.73 ppm for **L**[24]] (Fig. S5 and S6) and the slight displacement of the amidic proton signals in the ^{1}H-NMR spectra ($CDCl_3$) [δ_H = 9.36 ppm for **1**, 11.79 ppm for **2**, and 10.58 ppm for **L**[24]] (Fig. S7 and S8), clearly indicates that ligand **L** coordinates to the metal center(s) through the phosphorus atoms rather than through the nitrogen ones. X-ray diffraction analysis was carried out to confirm the structure of **1** and **2** and establish the coordination mode of **L** to the gold(I) center(s).

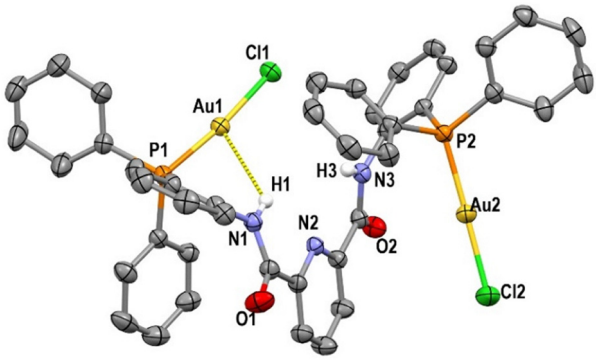

Fig. 1 Molecular structure of **1** with the labelling scheme for the atom positions. Hydrogen atoms, except those of the NH groups, have been omitted for clarity.

Crystals of **1** and **2**·1.5CH_2Cl_2, suitable for X-ray diffraction analysis, were obtained by slow diffusion of *n*-hexane into a saturated CH_2Cl_2 solution of the respective white solid samples at room temperature.

Regarding the crystal structure of compound **1** (Fig. 1 and Tables 1, 2), it features a gold(I) center coordinated to each phosphorous donor atom from ligand **L** [Au1–P1 = 2.2307(10) Å, Au2–P2 = 2.2266(11) Å], with a chloride ligand completing a linear coordination environment [Au1–Cl1 = 2.2718(11) Å, Au2–Cl2 = 2.2644(13) Å]. The polydentate ligand **L** thus acts as a bridge between the two metal centers. The molecule is not completely symmetrical, since one of the amide hydrogen atoms is involved in an intramolecular N–H···Au contact with one of the gold atoms [H1···Au1 = 2.977(48) Å, N1···Au1 = 3.5655(6) Å, N1–H1–Au1 = 146(5)°], whereas at the opposite end of the molecule the H3···Au2 distance of 3.44 Å and especially

Table 1 Selected bond distances (Å) and angles (°) in the crystal structures of **1** and **2**·1.5CH_2Cl_2

	1	**2**·1.5CH_2Cl_2
Au–P	2.2307(10) 2.2266(11)	2.3179(11) 2.3154(11)
Au–Cl/N	2.2718(11) 2.2644(13)	2.6424(12)
P–Au–Cl/N	173.10(4) 176.15(6)	101.26(4) 102.38(4)
P–Au–P		156.23(4)

Table 2 Hydrogen bonds features distances (Å) and angles (°) in the crystal structures of **1** and **2**·1.5CH_2Cl_2

	Contact	**1**	**2**·1.5CH_2Cl_2
Intramolecular N–H···Au	H···Au	2.977(48)	2.8345(1), 3.0316(1)
	N···Au	3.565(6)	3.461(4), 3.620(3)
	N–H···Au	146(5)	132.1, 127.4
Intramolecular N–H···Cl/C–H···O	H···Cl/O		2.635(2), 2.586(2)
	N···Cl/O		3.359(6), 3.325(4)
	N/C–H···Cl/O		142.4(4), 144.8(4)
1D	H···O	2.458(5), 2.409(5)	2.699(6), 2.605(5)
	C···O	3.388(9), 3.278(7)	3.468(12), 3.524(6)
	C–H···O	179.1(5), 155.6(4)	140.6(7), 169.5(5)
2D	H···Cl/O	2.842(2)	2.569(7)
	C···Cl/O	3.524(7)	3.429(14)
	C–H···Cl/O	131.1(4)	154.0(7)
3D	H···Cl		2.973(2)
	C···Cl		3.646(5)
	C–H···Cl		130.6(5)

the N–H···Au angle of 88° suggest the absence of any N–H···Au interaction.

This asymmetry is also reflected in the larger deviation from linearity at the gold(I) centre involved in the H···Au contact, where the P1–Au1–Cl1 angle is 173.10(4)°, compared to 176.15(6)° for the P2–Au2–Cl2 angle at the second metal centre. Neither intra- nor intermolecular Au···Au interactions are observed, while in the crystal packing, intermolecular C–H···O hydrogen bonds (Table 2 and Table S1) between adjacent units of **1** determine the formation of polymeric chains (Fig. S13A), and additional C–H···Cl hydrogen bonds (Table 2 and Table S1) that connect neighbouring chains result in the formation of a two-dimensional network (Fig. S13B).

To the best of our knowledge, N(amide)–H···Au(I) interactions have not so far been discussed in the literature. Furthermore, the experimental authentication of a genuine N–H···Au hydrogen bond (mainly involving amine groups) is a matter of ongoing debate.[18] With the exception of very few examples of gold(I) compounds exhibiting in their crystal structure intermolecular H···Au distances significantly shorter (below 2.5 Å)[13,18] than the sum of the corresponding van der Waals radii [Σ_{vdw}(H, Au) = 2.86 Å][25] and N–H–Au angles markedly higher than 110°,[13,18] whose bonding nature has also been supported experimentally by spectroscopic evidence, the vast majority of the reported cases claiming N–H···Au associations display H···Au separations close to the sum of the van der Waals radii (up to 3.0 Å) and N–H–Au angles in the range of 100–130°, with a maximum at around 113°. Often, even when supported by computational studies, the presence of other concomitant non-covalent interactions involving the gold(I) centre and/or the NH group casts some doubts on the genuine role these N–H···Au contacts play within the coordination environment of the metal centre.

To obtain more conclusive structural evidence for the possible and uncommon[13] N(amide)–H···Au(I) interaction observed in compound **1**, we investigated compound **2**, prepared from the reaction of **L** with one equivalent of [AuCl(tht)], in which the coordination of both phosphine donors to the same gold(I) centre is expected.

In fact, in the crystal structure of **2**·1.5CH_2Cl_2, the gold(I) centre is tri-coordinated by two phosphorus atoms from ligand **L** [Au–P1 = 2.3179(11) Å, Au–P2 = 2.3154(11) Å] and one chloride ligand [Au–Cl1 = 2.6424(12) Å], adopting a planar distorted T-shaped geometry (Fig. 2a). These Au–P and Au–Cl bond lengths are markedly longer than those observed in **1**, as a consequence of the different coordination environment around the gold(I) centre. Furthermore, the P–Au–Cl angles of 101.26(4)° [P1–Au–Cl1] and 102.38(4)° [P2–Au–Cl1] are significantly smaller than the P1–Au–P2 angle of 156.23(4)°, which lies halfway between those theoretically expected for trigonal-planar and linear coordination environments. This latter angle is much larger than that typically observed in gold(I) complexes featuring a coordination environment closer to trigonal planar and the same $AuClP_2$ fragment, in which longer Au–P and significantly shorter Au–Cl bond lengths are also generally recorded concurrently.[26–30]

It is worth noting that, due to the chelating coordination of **L**, the hydrogen atoms of the amide groups are both brought in close proximity to the gold(I) centre, with H···Au distances of 2.8345(1) Å and 3.0316(1) Å for H1···Au and H3···Au, respectively (see Table 2 and Table S2). Both hydrogens also engage in hydrogen bonding with the chloride ligand, showing H···Cl distances of 2.635(2) Å (H1···Cl1) and 2.586(2) (H3···Cl1) (Table 2 and Table S2). Compared to **2**·1.5CH_2Cl_2, in **1**, the N(amide)–H···Au(I) distance is intermediate between those found in **2**·1.5CH_2Cl_2, with H1···Au in the latter being slightly smaller than the sum of the van der Waals radii, while the N–H–Au angle is wider in **1** than in **2**·1.5CH_2Cl_2.

As in the crystal structure of **1**, no Au···Au interactions are observed in the crystal packing of **2**·1.5CH_2Cl_2; however, intermolecular hydrogen bonds of different natures are present. Thus, bifurcated C–H···O contacts involving O2 (Table 2 and Table S2) afford one-dimensional polymers that run parallel to the *b*-axis (Fig. S14A) that are connected through C–H···O hydrogen bonds involving O1 (Table 2 and Table S2), thus resulting in the formation of layers normal to the *c*-axis (Fig. S14B and C). Finally, these planes are joined *via* C–H···Cl hydrogen bonds (Table 2 and Table S2) that give rise to an extended 3D arrangement.

To eliminate any competitor of the amidic proton (particularly that from the chloride ligand) for the N(amide)–H···Au(I)

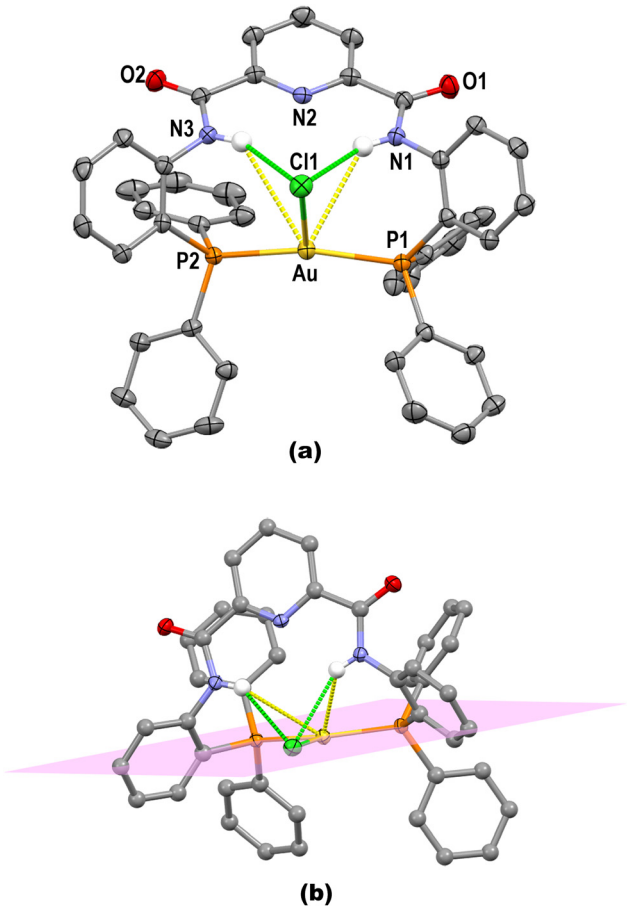

Fig. 2 (a) Molecular structure of **2**·1.5CH_2Cl_2 with the labelling scheme for the atom positions (the crystallization solvent molecules and hydrogen atoms, except those of the NH groups, have been omitted for clarity); and (b) alternative view of **2**·1.5CH_2Cl_2 showing the plane defined by the phosphorus and chloride donor atoms, as well as the position of the gold(I) center with respect to this plane.

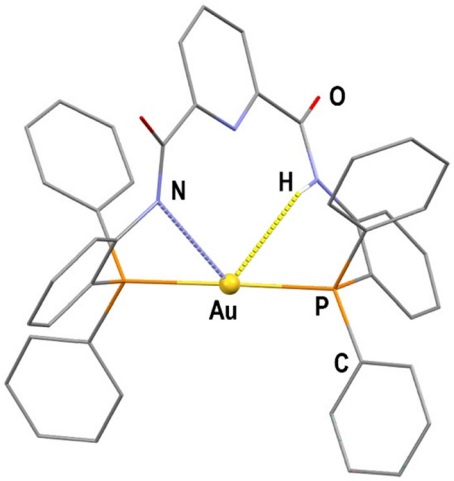

Fig. 3 Ligation at the gold(I) centre in Au($\mathbf{L}_{-H}$) (**3**).

interaction within a neutral gold(I) complex, compound **2** was treated with 1 equiv. of NaH in anhydrous THF, with the aim of deprotonating one amide group, thus forming an amidate anion, and simultaneously removing the chloride ligand. The reaction afforded a white solid denoted as [Au($\mathbf{L}_{-H}$)] (**3**), exhibiting limited stability and solubility properties comparable to those of **1** and **2**. Its molar conductivity in acetone solutions (5×10^{-4} M) was measured to be 3.0 Ω^{-1} cm^2 mol^{-1}, confirming its neutral character. Furthermore, compound **3** exhibits spectroscopic features (Fig. S9–S12) similar to those of **1** and **2**, including IR bands at 3196–2927 cm^{-1} [ν(N–H)] and a $^{31}P\{^1H\}$ NMR singlet at 32.98 ppm. Its ESI(+) mass spectrum shows the molecular ion peak at *m/z* 882.17, also found in the spectra of **1** and **2**. However, in compound **3**, the ^1H NMR signal corresponding to the single NH proton of the amide group, which would be expected for a neutral complex, could not be detected.

X-ray diffraction analysis was therefore carried out on single crystals obtained by slow diffusion of *n*-hexane into a saturated CH_2Cl_2 solution of the white solid. Due to the relative instability of the compound and the quality of the crystals, data collection had to be limited. Despite this limitation, the data still allow us to understand the nature of the compound, which is consistent with the expectations of the synthetic strategy. Although bond lengths and angles could not be determined with sufficient accuracy, the ligation at the metal centre can nevertheless be described, providing a proof of concept. The gold(I) centre is linearly coordinated to the two phosphorus atoms from ligand **L** (Fig. 3) with Au–P distances of about 2.3 Å. The asymmetric Au–N distances (of about 2.9 and 3.4 Å) facilitated the localization of the amide hydrogen atom, which participates in an intramolecular N(amide)–H···Au(I) interaction (H···Au = 2.6 Å, N···Au = 3.4 Å; N–H···Au = 140°), while the deprotonated nitrogen atom, with an Au–N distance of about only 2.9 Å establishes an unprecedented N(amidate)···Au(I) bonding interaction [Σ_{vdw}(N, Au) = 3.22 Å].[25] Therefore, the removal of the chloride ligand from the coordination sphere of gold(I) upon reaction of **2** with NaH seems to result in the strengthening of the N(amide)–H···Au(I) interaction, concomitant with the formation of a peculiar intramolecular N(amidate)···Au(I) bonding interaction. RCO(R′)N(amidate)–Au(I) bonds are well-known in the gold(I) coordination chemistry.[31–34] In all cases, the amidate anion plays a direct role in defining the linear coordination environment at the metal, exhibiting significantly shorter N–Au bond distances of around 2.0 Å. In **3**, N(amidate)···Au(I) and N(amide)–H···Au(I) interactions, although significantly shorter than the sum of van der Waals radii, act as secondary interactions at the metal centre, whose coordination environment is primarily defined by the two phosphine donors.

Hirshfeld surface analysis was performed to elucidate the dominant intermolecular interactions governing the crystal packing of complexes **1** and **2**. In both structures (see Fig. 4), the d_{norm} mapped surfaces display well-defined red spots associated with C–H···O hydrogen bonds, confirming that these contacts represent a common and significant stabilizing motif across the series. The reciprocal nature of these interactions is evident from the characteristic pair of sharp spikes observed in the corresponding 2D fingerprint plots, consistent with moderately strong C–H···O approaches. Complexes **1**

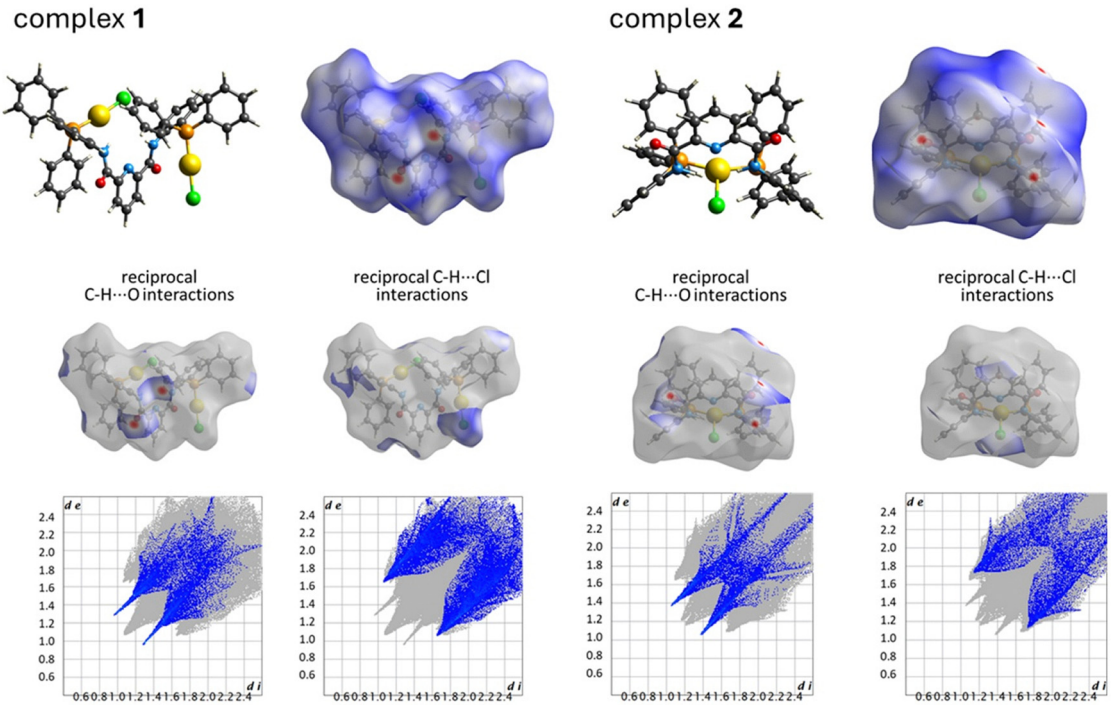

Fig. 4 Hirshfeld surface analysis (d_{norm}) and the associated 2D fingerprint plots for complexes **1** and **2**, highlighting the main intermolecular interactions.

and **2** also exhibit C–H···Cl contacts, although their manifestation on the Hirshfeld surface differs between the two systems. In complex **2**, a faint but discernible red region appears near the chloride atom, in line with the presence of short H···Cl approaches. In contrast, the structure of complex **1** displays intermolecular Cl···H distances below the sum of van der Waals radii, yet these interactions do not generate a red region on the d_{norm} surface, indicating that although geometrically short enough, they are less directional and weaker than those involving oxygen.

Computational studies

To support the structural evidence of a N(amide)–H···Au(I) hydrogen bond in **2** and **3**, we turned to analyse the electron-density in these complexes by performing non-covalent interaction (NCI) analysis of the electron density.[35] Model systems **2a** and **3a** were initially built up from the corresponding experimental X-ray structures, and fully optimized at the DFT PBE(D3)/def2TZVP level of theory,[36,37] including the empirical dispersion correction described by Grimme.[38]

The optimized geometrical parameters of **2a** and **3a** are very similar to those observed experimentally (Table S3) including different P–Au–P angles that depend on the gold(I) coordination environment, *i.e.*, three-coordinate and distorted trigonal planar in the case of **2a** and nearly linear and two-coordinate in the case of **3a**. In the case of model **2a,** two short NH···Cl stabilizing interactions are optimized, together with longer NH···Au and CH···Au contacts.

In the case of the asymmetric model **3a,** a markedly shorter NH···Au interaction is optimized at 2.66 Å, which is reinforced by the N(amidate)–Au(I) bonding interaction optimized at 2.99 Å, and several CH···Au contacts. These interactions were confirmed through NCI calculations and computation of the intrinsic bond strength index for weak interactions (IBSIW), which provide a relative comparison of the strength of stabilizing intramolecular interactions.

Fig. 5 and 6 depict the NCI isosurfaces for the two model systems, showing the spatial distribution of the non-covalent interaction densities in real space as coloured regions. The type of NCI can be determined semi-quantitatively by mapping the electron density multiplied by the sign of the second Hessian eigenvalue, sign(λ_2)ρ, onto the isosurfaces of the reduced density gradient $\sigma(r)$. When the sign of the second Hessian eigenvalue is positive ($\lambda_2 > 0$), red isosurfaces appear corresponding to steric and repulsive contacts. When the sign of the second Hessian eigenvalue is close to zero ($\lambda \approx 0$), green isosurfaces indicate van der Waals weak interactions. Conversely, when the sign of the second Hessian eigenvalue is negative

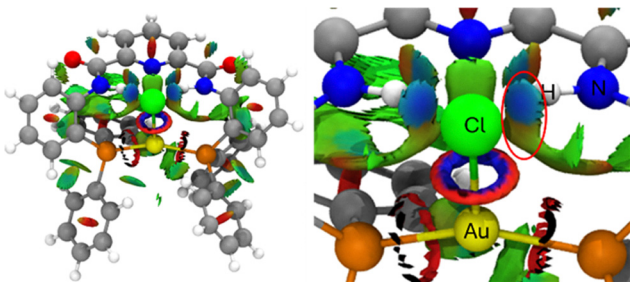

Fig. 5 NCI isosurface (isovalue = 0.5 a.u.) of the optimized model system **2a** (left) and detailed isosurface around the gold centre (left) showing the attractive nature of the N–H···Cl and N–H···Au interactions (red circle).

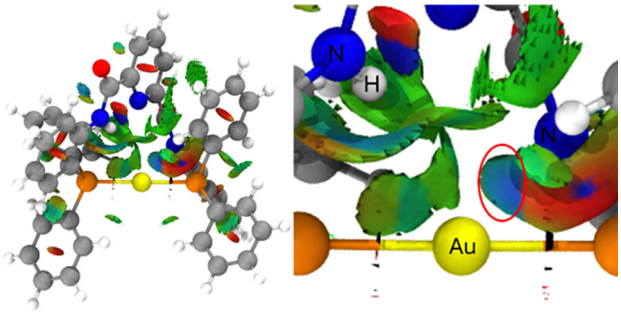

Fig. 6 NCI isosurface (isovalue = 0.5 a.u.) of the optimized model system **3a** (left) and detailed isosurface around the gold centre (left) showing the attractive nature of the N(amidate)···Au(I) interaction (red circle).

($\lambda_2 < 0$), green-blue or blue isosurfaces represent attractive NCIs. In the case of model **2a**, the strongest NCIs appear as bluish circles between the NH groups and the Cl atom.

In addition, below the bluish circles, the isosurface is extended as greenish regions indicating the presence of the expected N–H···Au interactions. In addition, other weak van der Waals interactions between the C–H groups of the phenyl rings also provide additional stabilizing interactions. In the case of model system **3a**, the strongest NCI is again depicted as a bluish region and represents the N(amidate)···Au(I) interaction. Green regions representing N–H···Au and C–H···Au van der Waals interactions are also displayed. The computed IBSIW indexes (Table S4) confirm that the N(amide)–H···Cl and N(amidate)···Au(I) interactions are attractive NCIs and represent the strongest ones in **2a** and **3a**, respectively. These are followed by the N(amide)–H···Au(I) interactions that are stronger in **3a** than in **2a**, as also inferred from the structural data.

Experimental

N,*N*′-bis{(2-diphenylphosphanyl)phenyl}-2,6-pyridinedicarboxamide (**L**)[23,24] and [AuCl(tht)] (CAS 39929-21-0) were prepared following the procedures reported in the literature. All reactions were conducted under a dry N_2 atmosphere, employing standard Schlenk techniques. Solvents were obtained from a solvent purification system (M-BRAUN MB SPS-800). Conductivity measurements were performed using a Jenway 4510 digital instrument (Jenway, Felsted, UK). Mass spectrometry data were acquired on a time-of-flight mass spectrometer equipped with an electrospray ionization (ESI) source (Bruker MicroTOF-Q spectrometer, Bruker Corporation, Bremen, Germany). The UATR-IR infrared spectra were recorded using a Perkin-Elmer 2 spectrophotometer equipped with a diamond crystal UATR attachment, covering a range of 4000–500 cm^{-1}. $^{31}P\{^1H\}$- and ^1H-NMR experiments were conducted on a Bruker AVANCE 400 spectrophotometer (Bruker Corporation, Fällanden, Switzerland) in $CDCl_3$ solutions. Chemical shifts are reported in ppm and referenced to H_3PO_4 (^{31}P, external) and $SiMe_4$ (^1H, external). Multiplicities are denoted as singlet (s), triplet (t) or multiplet (m).

Synthesis of [(L)(AuCl)$_2$] (1) and [(L)AuCl] (2). To a solution of **L** (0.1371 g, 0.2 mmol) in 20 mL of CH_2Cl_2 under an inert atmosphere, [AuCl(tht)] was added [0.1282 g (0.4 mmol) for the synthesis of **1**; 0.0641 g (0.2 mmol) for the synthesis of **2**]. The reaction mixture was stirred at room temperature for 6 hours. After this time, the solvent was partially evaporated under reduced pressure, and the addition of 20 mL of *n*-hexane induced the precipitation of a white solid. The resulting compound was collected by filtration, washed with *n*-hexane (3 × 1 mL), and dried under vacuum (97% yield for **1**; 48% yield for **2**). Crystals of **1** and **2**·1.5CH_2Cl_2 suitable for X-ray diffraction analysis were obtained by slow diffusion of *n*-hexane into a saturated CH_2Cl_2 solution of the compound at room temperature.

[(L)(AuCl)$_2$] (1). ^{1}H-NMR ($CDCl_3$, 298K), δ_H: 9.36 (s, 2H, H_1, NH), 8.07 (d, 2H, H_2, J = 7.48 Hz), 7.85 (t, 1H, H_3, J = 7.57 Hz), 7.71 (m, 2H, H_4), 7.55–7.38 (m, 14H, H_5, H_9, H_{10}), 7.33–7.31 ppm (m, 10H, H_6, H_8), 6.94–6.87 ppm (m, 2H, H_7) (see Fig. S7). $^{31}P\{^1H\}$-NMR ($CDCl_3$, 298K), δ_P: 23.98 ppm (s, PPh_2). UATR-IR: 3017–2946 (m, NH), 1739 (*vs.*, br, CO) 1685 (*vs.*, br, C-Hpy) cm^{-1}. ESI(+): *m*/*z* (%): 1114.1125 (55) [$C_{43}H_{33}Au_2ClN_3O_2P_2$] ([M–Cl]$^+$), 882.1760 (30) [$C_{43}H_{33}AuN_3O_2P_2$] ([M–Au–2Cl]$^+$), 375.17 (100) [$C_{19}H_{11}N_3O_2P_2$] ([L-4Ph-2H]$^+$). Λ_M (acetone, 5×10^{-4} M): 4.1 Ω^{-1} cm^2 mol^{-1}.

[(L)AuCl] (2). ^{1}H-NMR ($CDCl_3$, 298K), δ_H: 11.79 (s, 2H, H_1, NH), 8.10 (d, 2H, H_2, J = 7.5 Hz), 7.83 (t, 1H, H_3, J = 7.4 Hz), 7.74 (m, 2H, H_4), 7.54–7.39 (m, 14H, H_5, H_9, H_{10}), 7.33–7.28 ppm (m, 10H, H_6, H_8), 6.91–6.85 ppm (m, 2H, H_7) (see Fig. S8). $^{31}P\{^1H\}$-NMR ($CDCl_3$, 298K), δ_P: 34.97 ppm (s, PPh_2). UATR-IR: 3201–3055 (m, NH), 1738 (m, CO), 1682 (*vs.*, br, C-Hpy) cm^{-1}. ESI(+): *m*/*z* (%): 882.17 (100) [$C_{43}H_{33}AuN_3O_2P_2$]$^+$ ([M–Cl]$^+$). ESI(−): *m*/*z* (%): 915.92 (100) [$C_{43}H_{32}AuClN_3O_2P_2$]$^-$ ([M–H]$^-$). Λ_M (acetone, 5×10^{-4} M): 3.2 Ω^{-1} cm^2 mol^{-1}.

Synthesis of [Au(L$_{-H}$)] (3). To a solution of **L** (0.1377 g, 0.15 mmol) in anhydrous THF (10 mL) under an inert atmosphere, sodium hydride (NaH, CAS 7646-69-7, 6.0 mg, 0.25 mmol, 1.1 equivalents) was added. The resulting suspension was stirred at room temperature for 24 h, during which a cloudy, opaque solution formed. The reaction mixture was then filtered through a nylon syringe filter (0.45 µm, ∅ 25 mm) to remove any traces of unreacted NaH and the byproduct NaCl. The resulting filtrate was transferred to a second reaction flask under an inert atmosphere and dried under vacuum to afford the new complex as a white solid (42% yield). ^{1}H-NMR ($CDCl_3$, 298 K), δ_H: 8.48 (brd, 2H, H_4), 8.07 (d, 2H, H_2, J = 7.5 Hz), 7.65 (t, 1H, H_3, J = 7.54 Hz), 7.62–7.48 (m, 14H, H_5, H_9, H_{10}), 7.39–7.31 (m, 10H, H_6, H_8), 7.04–6.77 (m, 2H, H_7) (see Fig. S12). $^{31}P\{^1H\}$-NMR ($CDCl_3$, 298K), δ_P: 32.98 ppm (s, PPh_2). UATR-IR: 3196–2927 (m, NH), 1738 (*vs.*, br, CO), 1684 (*vs.*, br, C-Hpy) cm^{-1}. ESI(+): *m*/*z* (%): 882.17 (100) [$C_{43}H_{33}AuN_3O_2P_2$]$^+$ ([M]$^+$). Λ_M (acetone, 5×10^{-4} M): 3.0 Ω^{-1} cm^2 mol^{-1}.

Computational details. The model systems of complexes **2** and **3** (**2a** and **3a**, respectively) used in the computational studies were built up based on the X-ray diffraction results and fully optimized at the density functional theory (DFT) level employing the PBE functional,[36,37] along with the corresponding dispersion correction of Grimme,[38] as implemented in TURBOMOLE 6.4.[39] A topological analysis of non-covalent interactions (NCI) and IBSIW indexes for each model was

Table 3 Data collection and structure refinement details for **1** and **2**·1.5CH_2Cl_2

	1	**2**·1.5CH_2Cl_2
Chemical formula	$C_{43}H_{33}Au_2Cl_2N_3O_2P_2$	$C_{43}H_{33}AuClN_3O_2P_2$·1.5$CH_2Cl_2$
Crystal habit	Colourless	Colourless
Crystal size/mm	0.197 × 0.127 × 0.075	0.104 × 0.095 × 0.064
Crystal system	Triclinic	Monoclinic
Space group	$P\bar{1}$	$P2_1/c$
a/Å	11.1966(4)	13.6230(5)
b/Å	11.5477(4)	13.1182(5)
c/Å	16.5303(5)	25.1130(10)
α/°	90.624(1)	90
β/°	94.721(1)	99.3630(10)
γ/°	106.150(1)	90
V/Å^3	2044.70(12)	4428.1(3)
Z	2	4
Dc/g cm^{-3}	1.869	1.377
M	1150.49	918.127
F(000)	1096.1	1812.9
T/°C	23(2)	25(2)
2θmax/°	49.42	55.88
μ(Mo-Kα)/mm^{-1}	7.416	3.502
No. refl. Measured	51359	101847
No. unique refl.	6971	10570
R_{int}	0.0321	0.0629
$R[F > 2\sigma(F)]^a$	0.0205	0.0395
wR[F_2, all refl.]^b	0.0443	0.1000
No. of refl. used [$F > 2\sigma(F)$]	6971	10570
No. of parameters	545	488
No. of restrains	0	103
S^c	1.045	0.998
Max. residual electron density/e Å^{-3}	0.39	0.75

^{a} R: $(F) = \sum||F_o| - |F_c||/\sum|F_o|$. ^{b} w$R$: $(F^2) = [\sum\{w(F_o^2 - F_c^2)^2\}/\sum\{w(F_o^2)^2\}]^{0.5}$; $w^{-1} = \sigma^2(F_o^2) + (aP)^2 + bP$, where $P = [F_o^2 + 2F_c^2]/3$ and a and b are constants adjusted by the program. ^{c} $S = [\sum\{w(F_o^2 - F_c^2)^2\}/(n-p)]^{0.5}$, where n is the number of data and p is the number of parameters.

conducted using the Multiwfn software.[40] The electron density representations were generated using the VMD software for visualizing the results.[41]

Crystallography

Suitable single crystals were mounted in inert oil on a MiteGen MicroMount and transferred to the cold nitrogen stream of a Bruker APEX-II CCD area-detector diffractometer, equipped with an Oxford Instruments low-temperature controller system (Mo Kα = 0.71073 Å, graphite monochromator). Data were collected in ω- and φ-scan modes. Absorption effects were treated using numerical corrections. Complex **2** crystallizes with one and a half molecules of solvent per molecule of compound. The structures were solved with the XT structure solution program using intrinsic phasing and refined on F_0^2 with SHELXL-97.[42] All non-hydrogen atoms were treated anisotropically, and all hydrogen atoms were included as riding bodies except the amidic hydrogens in **1**, which were located in the Fourier map and refined freely (see Table 3). Hirshfeld isosurfaces and the corresponding fingerprint plots were generated using CrystalExplorer 21.[43]

Conclusions

This study provides new insights into the nature of weak NH···Au(I) interactions, a topic that remains under debate. Through the synthesis and characterization of a new series of gold(I) complexes with the pincer ligand *N*,*N*′-bis{(2-diphenylphosphanyl)phenyl}-2,6-pyridinedicarboxamide (**L**), it has been possible to explore the formation of rare examples of N(amide)H···Au(I) interactions in different coordination environments. In particular, in the neutral compound [Au($\mathbf{L}_{-H}$)] (**3**), beside an N(amide)H···Au(I) interaction exhibiting clear directionality and structural features consistent with a metal-centered hydrogen bond, an unprecedented secondary N(amidate)···Au(I) weak interaction is also observed, providing a valuable indication for further structural and computational investigations.

Author contributions

All authors contributed to the writing of the manuscript and approved its final version. The experimental work was conducted by L. C.-G., S. M., J. M. L.-L., M. E. O., C. C., G. P. and V. L., whereas the computational studies were performed by M. M.

Conflicts of interest

There are no conflicts to declare.

Data availability

The data supporting this article have been included as part of the supplementary information (SI). Supplementary

information: spectroscopic characterization, structural characterization and computational studies. See DOI: https://doi.org/10.1039/d6nj00558f.

CCDC 2525580 and 2525581 contain the supplementary crystallographic data for this paper.[44a,b]

Acknowledgements

We gratefully acknowledge the support from DGI MICINN/FEDER (project number PID2022-139739NB-l00 (AEI/FEDER, UE)) and from ''ERDF A way of making Europe''. L. C.-G. thanks the University of La Rioja for her predoctoral grant. We thank the Università degli Studi di Cagliari for financial support and the CeSAR (Centro Servizi d'Ateneo per la Ricerca) of the University of Cagliari.

Notes and references

1 E. Arunan, G. R. Desiraju, R. A. Klein, J. Sadlej, S. Scheiner, I. Alkorta, D. C. Clary, R. H. Crabtree, J. J. Dannenberg, P. Hobza, H. G. Kjaergaard, A. C. Legon, B. Mennucci and D. J. Nesbitt, Definition of the hydrogen bond (IUPAC Recommendations 2011), *Pure Appl. Chem.*, 2011, **83**, 1637–1641.

2 G. R. Desiraju, P. S. Ho, L. Kloo, A. C. Legon, R. Marquardt, P. Metrangolo, P. Politzer, G. Resnati and K. Rissanen, Definition of the halogen bond (IUPAC Recommendations 2013), *Pure Appl. Chem.*, 2013, **85**, 1711–1713.

3 C. B. Aakeroy, D. L. Bryce, G. R. Desiraju, A. Frontera, A. C. Legon, F. Nicotra, K. Rissanen, S. Scheiner, G. Terraneo, P. Metrangolo and G. Resnati, Definition of the Chalcogen bond (IUPAC Recommendations 2019), *Pure Appl. Chem.*, 2019, **91**, 1889–1892.

4 *Supramolecular Chemistry*, ed. J. W. Steed and J. L. Atwood, Wiley, 2009, ISBN: 9780470512333, DOI: 10.1002/9780470740880.

5 S. Hazra, D. Majumdar, D. Das, L. Barman, S. Roy and S. Dalai, A comprehensive review of the spodium bond as a new crystal engineering motif in Zn/Cd complexes: challenges and future perspectives, *Dalton Trans.*, 2026, **55**, 1584–1624.

6 M. Brookhart, M. L. H. Green and G. Parkin, Agostic interactions in transition metal compounds, *Proc. Natl. Acad. Sci. U. S. A.*, 2007, **104**, 6908–6914.

7 L. Brammer, Metals and hydrogen bonds, *Dalton Trans.*, 2003, 3145–3157.

8 A. Martín, Hydrogen bonds involving transition metal centers acting as proton acceptors, *J. Chem. Educ.*, 1999, **76**, 578–583.

9 A. S. K. Hashmi, Gold-Catalyzed Organic Reactions, *Chem. Rev.*, 2007, **107**, 3180–3211.

10 E. Jiménez-Nuñez and A. M. Echavarren, Gold-catalyzed cycloisomerizations of enynes: a mechanistic perspective, *Chem. Rev.*, 2008, **108**, 3326–3350.

11 A. Collado, D. J. Nelso and S. P. Nolan, Optimizing catalyst and reaction conditions in gold(I) catalysis–ligand development, *Chem. Rev.*, 2021, **121**, 8559–8612.

12 H. Schmidbaur, H. G. Raubenheimer and L. Dobrzańska, The gold-hydrogen bond, Au–H, and the hydrogen bond to gold, Au···H–X, *Chem. Soc. Rev.*, 2014, **43**, 345–380.

13 H. Schmidbaur, Proof of Concept for Hydrogen Bonding to Gold, Au···H–X, *Angew. Chem., Int. Ed.*, 2019, **58**, 5806–5809.

14 A. Sorroche, S. Moreno, M. El. Olmos, M. Monge and J. M. López-de-Luzuriaga, Deciphering the Primary Role of Au···H–X Hydrogen Bonding in Gold Catalysis, *Angew. Chem., Int. Ed.*, 2023, **62**, e202310314.

15 H. Nuss and M. Jansen, [Rb([18]crown-6)$(NH_3)_3$]Au NH_3: Gold as Acceptor in N–H···Au^- Hydrogen Bonds, *Angew. Chem., Int. Ed.*, 2006, **45**, 4369–4371.

16 L. Rocchigiani, W. T. Looster, S. J. Coles, D. L. Hughes, P. Hrobárik and M. Bochmann, Hydride Transfer to Gold: Yes or No? Exploring the Unexpected Versatility of Au···H−M Bonding in Heterobimetallic Dihydrides, *Chem. – Eur. J.*, 2020, **26**, 8267–8280.

17 M. Straka, E. Andris, J. Vícha, A. Růžička, J. Roithová and L. Rulíšek, Spectroscopic and Computational Evidence of Intramolecular Au^{I}···H^{+}−N Hydrogen Bonding, *Angew. Chem., Int. Ed.*, 2019, **58**, 2011–2016.

18 M. Rigoulet, S. Massou, E. D. Sosa Carrizo, S. Mallet-Ladeira, A. Amgoune, K. Miqueu and D. Bourissou, Evidence for genuine hydrogen bonding in gold(I) complexes, *Proc. Natl. Acad. Sci. U. S. A.*, 2019, **116**, 46–51.

19 F. Groenewald, J. Dillen, H. G. Raubenheimer and C. Esterhuysen, Preparing Gold(I) for Interactions with Proton Donors: The Elusive [Au]···HO Hydrogen Bond, *Angew. Chem., Int. Ed.*, 2016, **55**, 1694–1698.

20 M. A. Bakar, M. Sugiuchi, M. Iwasaki, Y. Shichibu and K. Konishi, Hydrogen bonds to Au in coordinated gold clusters, *Nat. Commun.*, 2017, **8**, 576.

21 R. J. F. Berger, J. Schoiber and U. Monkowius, A Relativity Enhanced, Medium-Strong Au(I)···H–N Hydrogen Bond in a Protonated Phenylpyridine-Gold(I) Thiolate, *Inorg. Chem.*, 2017, **56**, 956–961.

22 L. Coconubo-Guio, S. Moreno, M. Monge, M. E. Olmos and J. M. Lopéz-de-Luzuriaga, Gold(I) complexes of 2-(diphenylphosphino)aniline: synthesis and influence of the perhalophenyl ligand on their assembly, *Dalton Trans.*, 2025, **54**, 15923–15932.

23 E. K. van den Beuken, A. Meetsma, H. Kooijman, A. L. Spek and B. L. Feringa, New Palladium, platinum and nickel complexes based on rigid phosphorus and nitrogen ligands, *Inorg. Chim. Acta*, 1997, **264**, 171–183.

24 K.-C. Zhao, L. Liu, X.-C. Chen, Y.-Q. Yao, L. Guo, Y. Lu, X.-L. Zhao and Y. Liu, Multiple-Functional Diphosphines: Synthesis, Characterization, and Application to Pd-Catalyzed Alkoxycarbonylation of Alkyne, *Organometallics*, 2022, **41**, 750–760.

25 A. Bondi, Van der Waals Volumi and Radii, *J. Phys. Chem.*, 1964, **68**, 441–451.

26 G. A. Bowmaker, J. C. Dyason, P. C. Healy, L. M. Engelhardt, C. Pakawatchai and A. H. White, Lewis-base adducts of Group 11 metal(I) compounds. Part 27. Solid-state phosphorus-31 cross-polarization magic-angle spinning nuclear magnetic resonance, far-infrared, and structural studies on the mononuclear 2:1 adducts of triphenylphosphine with copper(I) and gold(I) halides, *J. Chem. Soc., Dalton Trans.*, 1987, 1089.

27 M. Hoshino, H. Uekusa, S. Ishii, T. Otsuka, Y. Kaizu, Y. Ozawa and K. Toriumi, Polymorphic Crystal Approach to Changing the Emission of $[AuCl(PPh_3)_2]$, Analyzed by Direct Observation of the Photoexcited Structures by X-ray Photocrystallography, *Inorg. Chem.*, 2010, **49**, 7257–7265.

28 H. Ito, T. Saito, T. Miyahara, C. Zhong and M. Sawamura, Gold(I) Hydride Intermediate in Catalysis: Dehydrogenative Alcohol Silylation Catalyzed by Gold(I) Complex, *Organometallics*, 2009, **28**, 4829–4840.

29 S. K. Mohapatra, S. Büschel, C. Daniliuc, P. G. Jones and M. Tamm, Selective Lithiation and Phosphane-Functionalization of $[(\eta^7\text{-}C_7H_7)Ti(\eta^5\text{-}C_5H_5)]$ (Troticene) and Its Use for the Preparation of Early-Late Heterobimetallic Complexes, *J. Am. Chem. Soc.*, 2009, **131**, 17014–17023.

30 S. Bestgen, M. T. Gamer, S. Lebedkin, M. M. Kappes and P. W. Roesky, Di- and Trinuclear Gold Complexes of Diphenylphosphinoethyl-Functionalised Imidazolium Salts and their N-Heterocyclic Carbenes: Synthesis and Photophysical Properties, *Chem. – Eur. J.*, 2015, **21**, 601–614.

31 R. S. Ramon, S. Gaillard, A. Poater, L. Cavallo, A. M. Z. Slawin and S. P. Nolan, $[\{Au(IPr)\}_2(\mu\text{-}OH)]X$ Complexes: Synthetic, Structural and Catalytic Studies, *Chem. – Eur. J.*, 2011, **17**, 1238–1246.

32 C. Jones, D. P. Mills, R. P. Rose, A. Stasch and W. D. Woodul, Synthesis and further reactivity studies of some transition metal gallyl complexes, *J. Organom. Chem.*, 2010, **695**, 2410–2417.

33 E. G. Perevalova, I. G. Bolesov, Y. S. Kalyuzhnaya, T. I. Voyevodskaya, L. G. Kuzmina, V. I. Korsunsky and K. I. Grandberg, Gold-containing derivatives of cyclopropanecarboxylic acid amides, *J. Organom. Chem.*, 1989, **369**, 267–280.

34 M. A. Cinellu, S. Stoccoro, G. Minghetti, A. L. Bandini and F. Demartin, Mono and dinuclear gold(I) complexes with neutral and deprotonated 1,4-benzodiazepin-2-ones. Crystal and molecular structure of $(L\text{-}H)Au(PPh_3)\cdot Et_2O$, where L = 1,3-dihydro-7-nitro-5-phenyl-2*H*-1,4-benzodiazepin-2-one, nitrazepam, *Inorg. Chim. Acta*, 1990, **168**, 33–41.

35 E. R. Johnson, S. Keinan, P. Mori-Sánchez, J. Contreras-García, A. J. Cohen and W. Yang, Revealing Noncovalent Interactions, *J. Am. Chem. Soc.*, 2010, **132**, 6498–6506.

36 R. G. Parr and W. Yang, *Density-Functional Theory of Atoms and Molecules*, Oxford University Press, New York, NY, USA, 1989.

37 C. Lee, W. Yang and R. G. Parr, Development of the Colle-Salvetti correlation-energy formula into a functional of the electron density, *Phys. Rev. B*, 1988, **37**, 785–789.

38 S. Grimme, J. Antony, S. Ehrlich and H. Krieg, A consistent and accurate *ab initio* parametrization of density functional dispersion correction (DFT-D) for the 94 elements H-Pu, *J. Chem. Phys.*, 2010, **132**, 154104.

39 R. Ahlrichs, M. Bär, M. Häser, H. Horn and C. Kölmel, Electronic structure calculations on workstation computers: The program system turbomole, *Chem. Phys. Lett.*, 1989, **162**, 165–169.

40 T. Lu and F. Chen, Multiwfn: A multifunctional wavefunction analyzer, *J. Comput. Chem.*, 2012, **33**, 580–592.

41 W. Humphrey, A. Dalke and K. Schulten, VMD: visual molecular dynamics, *J. Mol. Graphics*, 1996, **14**, 33–38.

42 G. M. Sheldrick, *SHELXL-97, Program for Crystal Structure Refinement*, University of Göttingen, Göttingen, Germany, 1997.

43 P. R. Spackman, M. J. Turner, J. J. McKinnon, S. K. Wolff, D. J. Grimwood, D. Jayatilaka and M. A. Spackman, *J. Appl. Cryst.*, 2021, **54**, 1006–1011.

44 (*a*) CCDC 2525580: Experimental Crystal Structure Determination, 2026, DOI: 10.5517/ccdc.csd.cc2qs2by; (*b*) CCDC 2525581: Experimental Crystal Structure Determination, 2026, DOI: 10.5517/ccdc.csd.cc2qs2cz.